Magnetic properties of the new diluted magnetic semiconductor $Zn_{1-x}Mn_xAs_2$: evidence of MnAs clusters

1999 J. Phys.: Condens. Matter 11 555

(http://iopscience.iop.org/0953-8984/11/2/018)

J. Phys.: Condens. Matter **11** (1999) 555–568. Printed in the UK PII: S0953-8984(99)88321-0

Magnetic properties of the new diluted magnetic semiconductor $Zn_{1-x}Mn_xAs_2$: evidence of MnAs clusters

R Laiho†, K G Lisunov†‡, E Lähderanta† and V S Zakhvalinskii†‡
† Wihuri Physical Laboratory, University of Turku, FIN-20014 Turku, Finland
‡ Institute of Applied Physics, Academiei str. 5, MD-2028 Kishinev, Moldova

Received 10 October 1997, in final form 22 September 1998

Abstract. The preparation and magnetic properties of the diluted magnetic semiconductor $Zn_{1-x}Mn_xAs_2$, opening a novel group of II–V_2 compounds alloyed with transition metal elements, are reported for the first time. Single crystals of $Zn_{1-x}Mn_xAs_2$ are obtained with a modified Bridgman method. For $x \leqslant 0.2$ their structure is isomorphic to the $ZnAs_2$ parent compound. Magnetic properties of $Zn_{1-x}Mn_xAs_2$ are investigated for $x = 0.01$, 0.05 and 0.1 between $T = 2$ and 500 K in fields up to 60 kG. All the samples show a steep decrease of magnetization well above 300 K. In low fields (2–200 G) the temperature dependence of the magnetic susceptibility is strongly irreversible below $T_b \approx 250$ K. The magnetization displays nonlinear field dependence starting from $B \sim 1$–2 kG and reaching full saturation above 40 kG. Its temperature dependence is weak between 2 and 300 K. The magnetic properties are explained by the presence of MnAs clusters. The distribution of cluster sizes is described by three overlapping Gaussian functions with the maxima at 1.7, 2.4 and 3.3 nm. At 300 K the corresponding magnetic moments are found to be 1.5, 4.1 and 10.4 in units of $10^3\ \mu_B$.

1. Introduction

A small amount of transition metal element (Mn, Fe or Co) incorporated in a non-magnetic semiconductor matrix has usually a strong influence on its magnetic, optical and transport properties [1]. Such materials, or diluted magnetic semiconductors (DMSs), have interactions not present in the parent compounds. Among them is the s–d exchange interaction between band carriers and localized magnetic moments of the transition metal ions and the d–d interaction between the ions themselves. The best known DMSs belong to the II–VI and IV–VI groups. Their properties are reviewed e.g. in [1] and [2]. For a long time these materials have been regarded as typical representatives of DMSs, giving minor attention to other diluted systems. On the other hand, in recent investigations of II_3V_2 ternary, $(Cd_{1-x}Mn_x)_3As_2$ and $(Zn_{1-x}Mn_x)_3As_2$, and quaternary, $(Cd_{1-x-y}Zn_xMn_y)_3As_2$, compound alloys [3–7] unusual phenomena not observed earlier in the II–VI and IV–VI DMSs were discovered. Among them are coexistence of two spin-freezing effects, one at a low ($T < 4$ K) [3, 4] and the other at a high ($T \sim 200$ K) [5–7] temperature in one and the same material, anomalous low-temperature electronic properties [8] and strong dependence of the electron effective mass on the applied magnetic field [9, 10].

However, the group of the II–V semiconductors is much larger than the group of the II_3V_2 compounds containing the materials mentioned above.The unusual properties of the latter stimulate interest to find new DMSs among other II–V compounds. In this work we report our effort to extend the group of DMSs to II–V_2 semiconductors and communicate results of the first investigations of the new alloys $Zn_{1-x}Mn_xAs_2$.

0953-8984/99/020555+14$19.50

2. Preparation of the crystals

2.1. Properties of the $ZnAs_2$ host material

$Zn_{1-x}Mn_xAs_2$ can be obtained by substituting Mn for Zn in $ZnAs_2$. The properties of the host material are reviewed in [11]. In particular, the crystal structure of $ZnAs_2$ belongs to the β-ZnP_2 type (space group $P2_1/c$, or C_{2h}^5) having eight formula units in the unit cell with the parameters $a = 9.287$ Å, $b = 7.61$ Å, $c = 8.01$ Å and $\beta = 102.5^\circ$ [12]. However, the structure of $ZnAs_2$ differs from that of β-ZnP_2 by the absence of Zn–Zn bonds. Along with Zn–As bonds also As–As bonds are present. The As atoms form chains along the $\boldsymbol{c}$-axis which are connected with Zn atoms [11]. Electronic properties of $ZnAs_2$ are governed by the relatively wide band gap (0.9 eV) and impurities or intrinsic defects. Undoped crystals are p-type semiconductors with hole concentration $p = 10^{14}$–10^{16} cm^{-3} [13, 14] at 300 K. By doping with Se or Te [14] the p-type conduction can be changed to n-type with electron concentration $n = 8 \times 10^{16}$ cm^{-3} [14]. The anisotropic structure of $ZnAs_2$ leads to the dependence of certain physical quantities on the crystal direction, e.g. the Hall coefficient $R_{[100]}/R_{[001]} = 5$ and the resistivity $\rho_{[100]}/\rho_{[001]} = 100$ [15].

2.2. Preparation and characterization of $Zn_{1-x}Mn_xAs_2$

First we investigated the interval of forming $Zn_{1-x}Mn_xAs_2$ solid solutions within the system of $ZnAs_2$–$MnAs_2$ alloys. The samples were synthesized in the interval of $0 \leqslant x \leqslant 0.5$ using the modified Bridgman method (slow cooling of a melt in the presence of a temperature gradient in a furnace). Stoichiometric amounts of Zn, Mn and As (99.999% purity) were mixed and put into a quartz ampoule after covering its inner wall with a layer of carbon. The synthesis was performed in vacuum at 1000 °C (the melting point of $ZnAs_2$ is 771 °C) by cooling the material down to 800 °C at the speed of 50 °C h^{-1} and further to 700 °C at the speed of 10 °C h^{-1}. The polycrystalline ingots were analysed with x-ray powder diffraction measurements. A monoclinic structure (space group $P2_1/c$, or C_{2h}^5) with $z = 8$ and lattice parameters $a = 9.28$ Å, $b = 7.68$ Å, $c = 8.03$ Å and $\beta = 102.3^\circ$ was identified unambiguously for $x = 0.3$. The positions of the diffraction peaks correspond well with those of $ZnAs_2$. Incorporation of Mn in the lattice was revealed by the clearly observed x-ray fluorescence background and by variations in the intensities of the x-ray diffraction lines. Generally, the applied powder diffraction method allowed the phase analysis of the system $ZnAs_2$–$MnAs_2$ in the interval of $0 \leqslant x \leqslant 0.5$ establishing the upper boundary for existence of $Zn_{1-x}Mn_xAs_2$ solid solutions as $x \approx 0.2$–0.3. No dependence of the lattice parameters on the composition could be established.

Single crystals of $Zn_{1-x}Mn_xAs_2$ were grown in the interval of $x = 0$–0.2 by increasing the amount of the starting materials, prolonging the time of the synthesis at 1000 °C to 20 h and decreasing the cooling rate in the domain of crystallization down to 1.5–2 °C h^{-1}. X-ray analysis showed good agreement with the results obtained for the polycrystalline ingots and interplane distance in a satisfactory agreement with that of $ZnAs_2$. This shows that substitution of Zn for Mn in $ZnAs_2$ practically does not distort the $ZnAs_2$ type crystal structure up to $x = 0.2$. No trace of a second phase could be detected within this interval of the composition. The concentrations of Zn, Mn and As in the ingots were controlled by weighing the amounts of the starting materials with accuracy of 0.001%. No material fractions or traces of volatile components could be found inside the crucible containing the ingot. X-ray phase analysis gave the same diffraction line patterns for specimens prepared from different parts of the ingots having $x \leqslant 0.2$. This brings the error in determination of x close to that of the x-ray analysis, about 1.5%. At higher values of x weak peaks due to an impurity phase were found

in polycrystalline samples of the system. Small single crystals of As were segregated from this phase in some ingots with x between 0.3–0.5.

3. Magnetic measurements

Dc magnetic measurements were made between 2 and 300 K with a SQUID magnetometer using unoriented $Zn_{1-x}Mn_xAs_2$ crystals with $x = 0.01$, 0.05 and 0.1, and an oriented specimen with $x = 0.05$. The values of $x \leqslant 0.1$ were chosen below and far enough from the upper boundary of the interval of the solid solutions. The temperature of the sample was controlled with flowing helium gas. Before every measurement the sample was annealed for 1.5–3 h at 140 °C to avoid the influence of possible remanent magnetization.

The temperature dependence of the magnetization, $M(T)$, in weak (2–200 G) and moderate (0.2–10 kG) fields was measured after cooling the sample in zero ($B < 0.1$ G) field (ZFC) from 300 to 2 K or while cooling it in a field (FC). As can be seen from figure 1 the plots of $\chi_{ZFC}(T)$ and $\chi_{FC}(T)$ ($\chi = M/B$) measured in low fields diverge clearly in the region of $T \lesssim 300$ K. Additionally, $\chi_{ZFC}(T)$ has a broad maximum around $T_b \approx 250$ K. The difference between $\chi_{ZFC}(T)$ and $\chi_{FC}(T)$ decreases strongly on increasing the field of the measurement in the interval of 2–200 G (for convenience the plots in figure 1 are presented so that their $\chi_{FC}(T)$ parts coincide with the $\chi_{FC}(T)$ measured at $B = 2$ G). The observed irreversibility is suppressed as B is increased up to 0.5–0.7 kG and disappears completely above 2 kG.

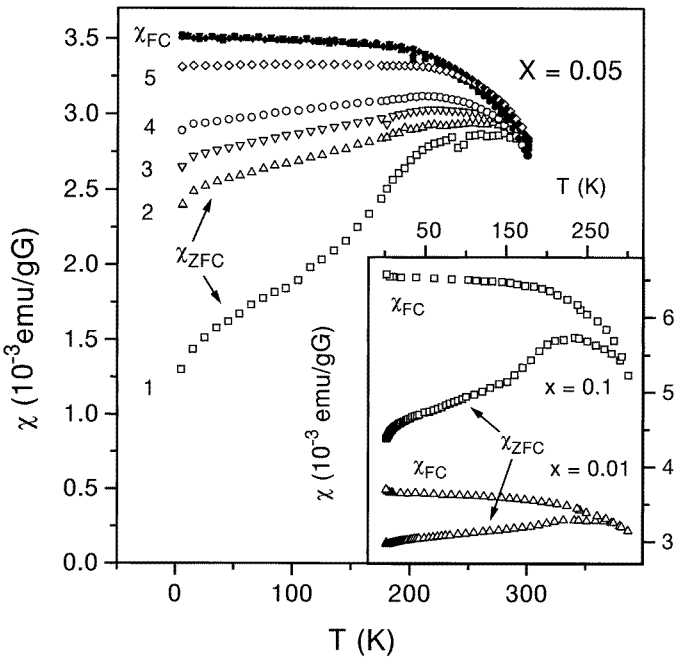

Figure 1. Temperature dependences of χ_{ZFC} (open symbols) and χ_{FC} (closed symbols) for $Zn_{1-x}Mn_xAs_2$ with $x = 0.05$, measured at $B = 2$ G (1), 5 G (2), 20 G (3), 50 G (4) and 200 G (5). The scale of the χ-axis corresponds to χ_{ZFC} and χ_{FC} for $B = 2$ G. The other plots are shifted so that their FC parts coincide with that for $B = 2$ G. Inset: χ_{ZFC} and χ_{FC} against T for samples with $x = 0.01$ and 0.1, measured in the field of 10 G.

In figure 2 is displayed the magnetic field dependence of the magnetization, $M(B)$, at different temperatures for the sample with the Mn concentration $x = 0.01$, and in figure 3 for that with $x = 0.05$. The magnetization increases at first very rapidly with increasing field but starts to deviate from a linear growth at $B \approx 1$–2 kG. In the sample with $x = 0.01$ it reaches a broad maximum around $B_{max} \approx 20$–30 kG but this maximum is not observed when x is increased to 0.05. The temperature dependence of the magnetization between 2 and 200 K is quite weak. A measurable difference of the magnetization for the specimen with $x = 0.05$ and the field oriented perpendicular and parallel to the (100) plane is evident from figure 4.

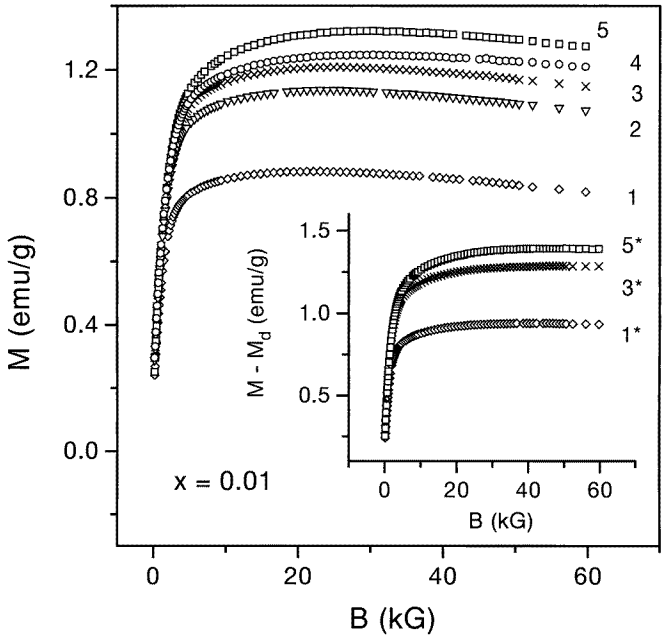

Figure 2. Dependence of the magnetization of $Zn_{1-x}Mn_xAs_2$ on the magnetic field for $x = 0.01$ and $T = 300$ K (1), 200 K (2), 100 K (3), 20 K (4) and 2 K (5). Inset: magnetic field dependence of the magnetization corrected by subtracting the diamagnetic contribution (M_d) for the same specimen and $T = 300$ K (1*), 100 K (3*) and 2 K (5*).

To complete the picture above we have investigated the temperature dependence of the susceptibility, χ, between 250 and 500 K for $B = 20$ G, 200 G, 2 kG and 60 kG. As can be seen from figure 5 both $\chi_{ZFC}(T)$ and $\chi_{FC}(T)$ decrease strongly in the temperature region above 300 K suggesting a ferromagnetic (FM) transition in the specimen with $x = 0.01$. The transition temperature, T_C, increases when B is increased. Additionally, the measurements in the field of $B = 60$ kG (squares) show that at $T \geqslant 370$ K the susceptibility is negative and that above 410 K it becomes roughly independent of temperature, demonstrating the presence of a diamagnetic contribution, M_d, in the magnetization of this sample. Subtraction of M_d leads to disappearance of the maxima in the $M(B)$ curves (see the inset to figure 2). For the specimens with $x = 0.05$ and 0.1 a similar transition is observed (see figure 6), with T_C being close to that of the sample with $x = 0.01$.

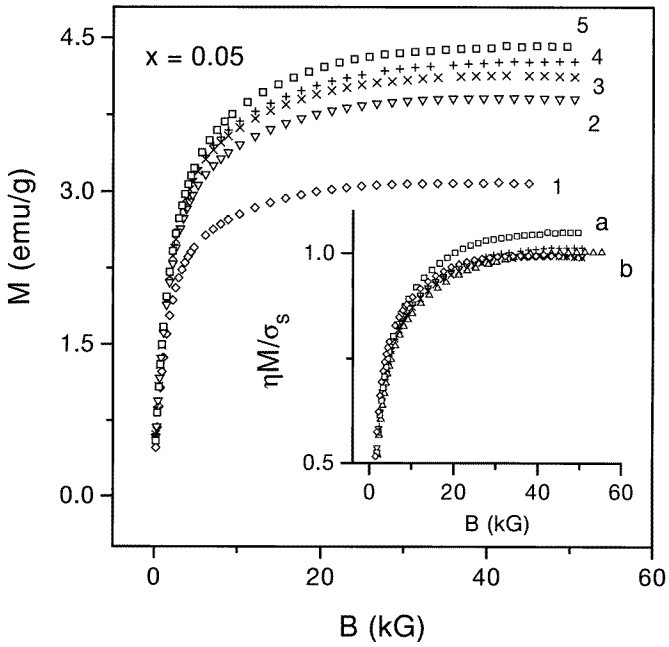

Figure 3. Dependence of the magnetization of $Zn_{1-x}Mn_xAs_2$ for $x = 0.05$ on the magnetic field for $x = 0.05$ and $T = 300$ K (1), 200 K (2), 100 K (3), 20 K (4) and 2 K (5). Inset: $\eta M/\sigma_s$ against B for $T = 1.9$ K (a) and $T = 20$ K, 50 K, 100 K, 200 K and 300 K (b).

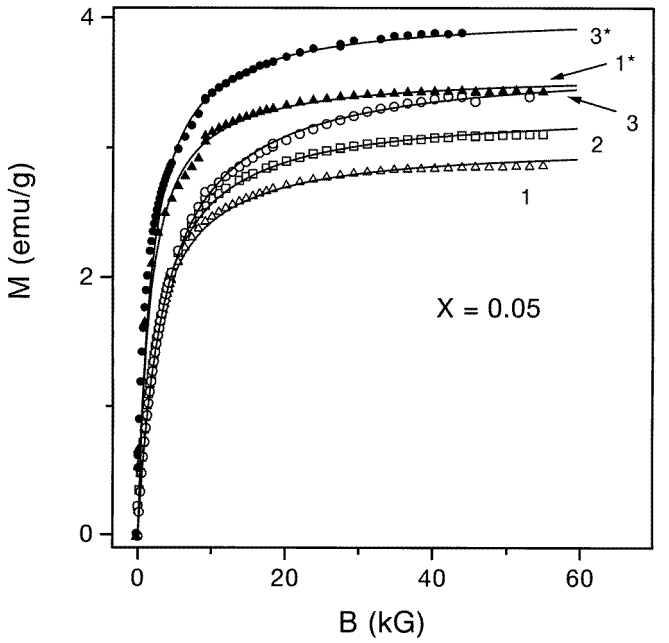

Figure 4. Dependence of the magnetization of $Zn_{1-x}Mn_xAs_2$ ($x = 0.05$) on the magnetic field for $B \parallel (100)$ at $T = 200$ K (1), 50 K (2) and 5 K (3) and $B \perp (100)$ at $T = 200$ K (1^*) and 5 K (3^*). The solid lines are fits with equation (4).

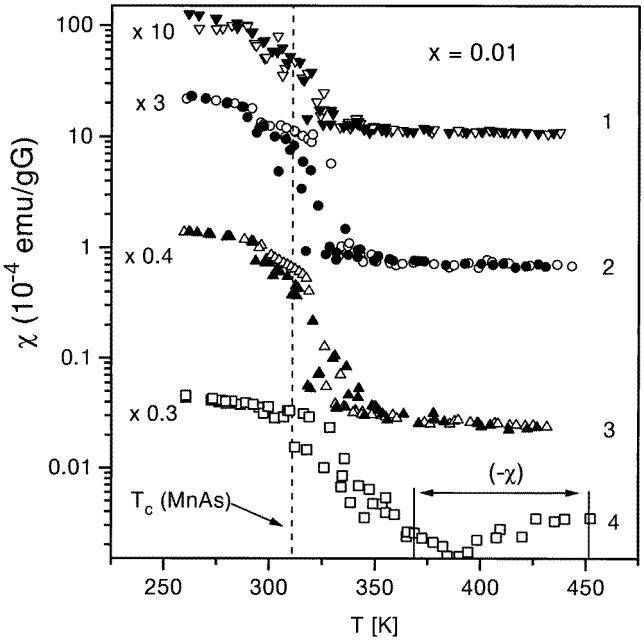

Figure 5. Susceptibility against temperature in $Zn_{1-x}Mn_xAs_2$ for $x = 0.01$ and $B = 20$ G (1), 200 G (2), 2 kG (3) and 60 kG (4). The open and the closed symbols represent χ_{ZFC} and χ_{FC}, respectively. The dashed line indicates the Curie temperature of MnAs.

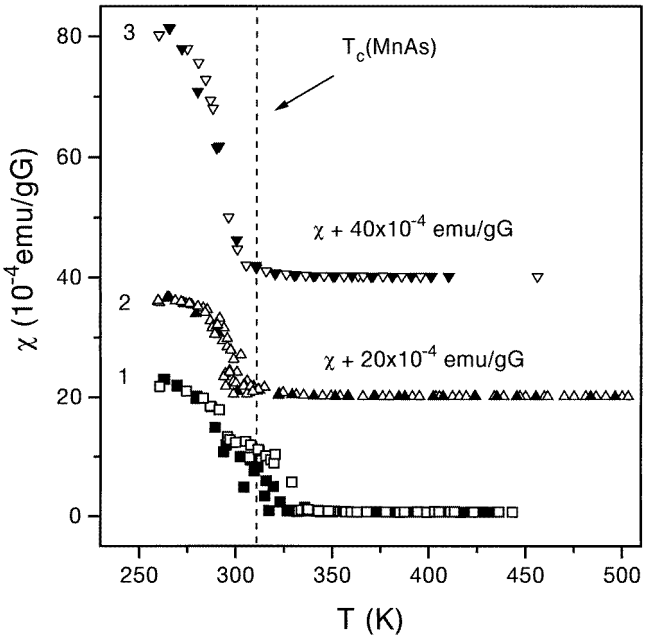

Figure 6. Susceptibility against temperature in $Zn_{1-x}Mn_xAs_2$ for $x = 0.01$ (1), 0.05 (2) and 0.1 (3) and $B = 200$ G. The open and the closed symbols represent χ_{ZFC} and χ_{FC}, respectively. The dashed line exhibits the Curie temperature of MnAs. For convenience the data (2) and (3) are shifted along the χ axis by the amounts shown above the corresponding curves.

4. Discussion

The magnetic properties of $Zn_{1-x}Mn_xAs_2$ described above give strong evidence for presence of small FM clusters of MnAs in all the samples investigated. Above $T_D = 394$ K bulk MnAs has hexagonal $B8_1$ (NiAs-type) structure and below T_D the orthorhombic B31 (MnP-type) structure. Both these phases are paramagnetic (PM) [16]. At $T_{Cc} \approx 306$ K (on cooling in a zero field) a first-order magnetostructural phase transition takes place whereupon the hexagonal modification $B8_1$ is while spontaneous (FM) magnetization, $\sigma_s(T)$, appears. On heating at $B = 0$ σ_s vanishes at $T_{Ch} \approx 317$ K [16]. The average temperature of T_{Cc} and T_{Ch} for MnAs is shown by the dashed line in figures 5 and 6. The values of T_C in the investigated $Zn_{1-x}Mn_xAs_2$ specimens are close to this line. When B is increased from 0 to 60 kG T_{Ch} and T_{Cc} are shifted to higher temperatures by about 20 and 30 K, respectively [16]. A similar shift of T_C is observed between 20 G and 60 kG in $Zn_{1-x}Mn_xAs_2$ with $x = 0.01$ (figure 5). It is worth mentioning that the steep decrease of magnetization at $T_{IC} \approx 310$ K indicating the presence of MnAs clusters was observed recently in the III–V DMS $In_{0.82}Mn_{0.18}As$ [17].

From the difference between the magnetization of $Zn_{1-x}Mn_xAs_2$ at $T \lesssim T_C$ and $T \gtrsim T_C$ and the value of $\sigma_s = 630$ emu cm^{-3} (300 K) [18] the volume fraction, η, of MnAs was estimated to be 0.023 and 0.035 for the samples with $x = 0.05$ and 0.10, respectively, and less than 0.005 for that with $x = 0.01$. This corresponds to fractions $\beta = 0.97$ and 0.73 of the total amount of Mn entering the MnAs clusters in $Zn_{1-x}Mn_xAs_2$ for $y = 0.05$ and 0.10, respectively. The values of η lie definitely beyond the sensitivity of the x-ray analysis. Since the overwhelming majority of Mn ions is located in the clusters no regular dependence of the lattice parameters on composition is expected, in agreement with our observations.

For a detailed analysis over extended temperature regions on both sides of T_C it is convenient to choose the sample with $x = 0.05$, because the amount of free (i.e. not entering the clusters) Mn ions in this sample is estimated to be much smaller than in the specimen with $x = 0.10$ and the diamagnetic contribution to the net magnetization is negligible compared with the specimen having $x = 0.01$. The latter is evident from (i) the absence of the maxima in the $M(B)$ curves (cf figures 3 and 4 and figure 2) in the sample with $x = 0.05$ and (ii) the fact that the negative susceptibility (figure 5) is observed in our experiments only in the specimen with $x = 0.01$.

In figure 7 is shown the saturation magnetization, M_s, of $Zn_{1-x}Mn_xAs_2$ (triangles) along with the dependence of σ_s on T for MnAs [18] extrapolated to $T = 0$ and multiplied by the factor of $\eta = 0.023$ (dashed line). The functions $M_s(T)$ and $\eta\sigma_s(T)$ coincide down to $T \approx 50$ K. Hence, the volume fraction of MnAs in $Zn_{1-x}Mn_xAs_2$ and, consequently, the fraction of Mn ions in MnAs, $\beta = 0.97$, are the same with those obtained above from the data in the vicinity of T_C. Suggesting that the deviation of $M_s(T)$ from $\eta\sigma_s(T)$ below 50 K is due to a PM contribution, $M_p(T)$, of the free Mn ions, we fit $M_s(T)$ between $T = 2$ and 300 K with the sum of $\eta\sigma_s(T) + M_p(T)$. Here $M_p(T) \approx \chi_p(T)B^*$ with $B^* \approx 40$ kG being the field where the contribution of the MnAs clusters to the net magnetization is practically saturated while that of the free Mn ions is still sufficiently far from saturation and can be approximated reasonably with a linear function. The susceptibility $\chi_p(T)$ satisfies the Curie–Weiss law

$$\chi_p(T) = C_1/(T - \theta_1). \tag{1}$$

In equation (1) $C_1 = p_{eff}^2\mu_B^2 N_f/3k_B$ is the Curie constant, p_{eff} is the effective number of Bohr magnetons per free Mn ion, N_f is their concentration and θ_1 is the Curie–Weiss temperature determined by the interaction between the free Mn ions. From the best fit with the observed data of $M_s(T)$ we obtain $C_1 = 1.3 \times 10^{-4}$ emu K cm^{-3} G^{-1} and $\theta_1 = -4.2$ K. The negative sign of θ_1 implies that the interaction between the free Mn ions in $Zn_{1-x}Mn_xAs_2$ is

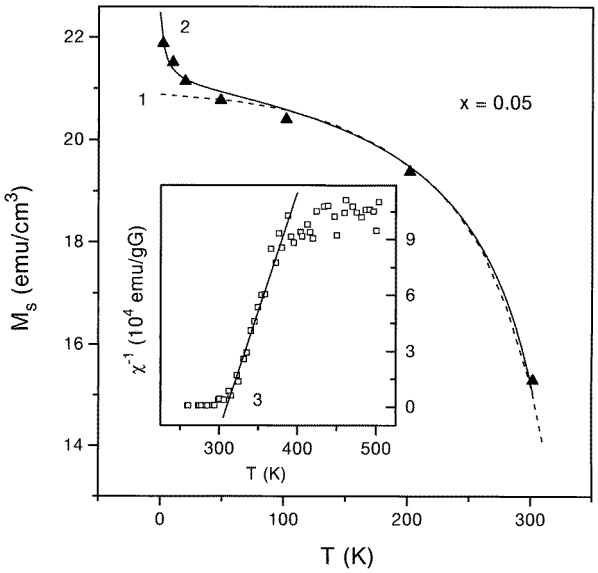

Figure 7. Temperature dependence of the saturation magnetization of $Zn_{1-x}Mn_xAs_2$ for $x = 0.05$ (triangles) compared with the reduced saturation magnetization of MnAs $\eta\sigma_s$ (line 1) and the sum of $\eta\sigma_s$ and the PM contribution of free Mn ions (line 2). Inset: temperature dependence of the inverse susceptibility above T_C.

antiferromagnetic (AF) as in all known DMSs containing Mn. With $p_{eff} = 35$ for Mn^{2+} we obtain $N_f = 1.8 \times 10^{19}$ cm^{-3} and the fraction of free Mn ions, 0.026, corresponding to $\beta = 0.974$ which agrees very well with the value of β obtained above in the interval of 50–300 K and for $T \gtrsim T_C$. We conclude, that the temperature dependence of the saturation magnetization in $Zn_{1-x}Mn_xAs_2$ is most probably determined by that of the MnAs clusters with minor influence of the free Mn ions below 50 K.

At temperatures above T_C, namely between 320 and 380 K, the susceptibility exhibits the Curie–Weiss law again (see the inset to figure 7) but with other values of the Curie–Weiss temperature, $\theta_2 = 310 \pm 20$ K, and the Curie constant, $C_2 = (3.3 \pm 0.3) \times 10^{-3}$ emu K cm^{-3} G^{-1} corresponding to $p_{eff} = 4.8 \pm 0.4$ per Mn ion. These values coincide within the experimental error with $\theta = 285$ K and $p_{eff} = 4.45$ in the PM hexagonal phase of bulk MnAs [16] existing above 394 K. In bulk MnAs the width of the orthorhombic phase is 80–90 K. As follows from the shift of T_C with B, about 30 K (figure 6), in the sample with $x = 0.01$ and from the value of $T_C \gtrsim 300$ K and the onset of the Curie–Weiss law ($\sim$320 K, figure 7) in the sample with $x = 0.05$ it does not exceed $\sim$20–30 K in MnAs clusters of $Zn_{1-x}Mn_xAs_2$.

The above discussion gives sufficient evidence that the magnetic properties of $Zn_{1-x}Mn_xAs_2$ are determined mostly by small ferromagnetic MnAs clusters. Generally, small single domain FM particles incorporated in a solid matrix can exist in two different states [19]. At $T > T_b$ or above the blocking temperature thermal fluctuations can cause a sort of Brownian rotation of the magnetic moment of the particles with the result that an assembly of such particles exhibits superparamagnetic (SP) behaviour. In this case M, corrected against the temperature dependence of the saturation magnetization of the clusters, would be a Langevin-type function of the ratio B/T. At $T < T_b$ the moments of the particles are blocked, with their directions distributed at random over the sample volume violating the B/T-scaling of M. There are two conceivable sources of the blocking barriers: (i) the

anisotropy energy of individual particles and (ii) the dipolar interaction between the moments of different particles.

In the case (i) the moment of each particle is stabilized independently when its anisotropy energy, KV, becomes high enough to counteract the thermal excitations $\sim k_B T$. Here K is the density of the anisotropy energy and V is the volume of the particle. After removal of the external field the moments of the particles relax towards an equilibrium state. The relaxation time, τ, is given by $1/\tau = f_0 \exp(-KV/k_B T)$, where f_0 is a frequency factor of the order of 10^9 s^{-1}. When the value of $\tau = 10^2$ s is used as the criterion for transition to stable behaviour the energy barrier must be $25\, k_B T$. Then the blocking temperature can be written as [19]

$$T_b^{(anis)} = KV/25\, k_B. \tag{2}$$

The temperature dependence of M is determined only by that of the saturation magnetization of the FM particles, σ_s, so that the ratio M/σ_s would be temperature independent.

In case (ii) the blocking temperature and the magnetization will satisfy the equations (see equation (A10) and (A11) in appendix A)

$$T_b^{(inter)} = \mu^2 I_0^{1/2}/3\, k_B \tag{3}$$

and

$$M = M_s B/(B + \xi M_s) \tag{4}$$

respectively. In equation (4) $M_s = \mu N$ is the saturation magnetization of the specimen, μ and N are the moment and the concentration of the particles (neglecting the distribution of their sizes), $I_0 = z_I/r^6$, $z_I = 11.6$, $r = 2(4\pi N/3)^{-1/3}$ is the mean distance between particles and $\xi = 17.3$.

The blocking transition (i.e. transition from the SP to stable behaviour) of the assembly of single-domain particles can be identified by deviation of $\chi_{ZFC}(T)$ from $\chi_{FC}(T)$. The blocking temperature T_b is defined by the cusp of χ_{ZFC}(T) meaning that for $T > T_b$ the thermal energy is large enough to enable the clusters to be oriented by an external magnetic field. Below T_b clusters cannot overcome the blocking barriers (independent of their nature) [19] with the help of thermal excitations. Blocking temperatures as high as the room temperature were established e.g. in heterogeneous metallic Cu–Co alloy films containing nanometre scale FM Co-rich clusters [20] and in III–V semiconductor GaAs with Fe_3GaAs precipitates [21]. Lower values of T_b were observed in some granular systems demonstrating SP response of the clusters and related giant magnetoresistance (see [21] and references therein). Accordingly, the high-temperature irreversible phenomena shown in figure 1 can be attributed to the presence and blocking of the MnAs cluster moments in the samples. It is interesting to note that the blocking transition is broad in $Zn_{1-x}Mn_xAs_2$ and overlaps with the transition from PM to FM state in MnAs clusters (cf figures 1, 5 and 6). Consequently, the SP region corresponding to unstable cluster moments is practically unobservable.

As evident from figure 3 the ratio of M/σ_s is in all fields independent of T within the error of 2–3%, excluding the data at 2 K which are influenced by increasing PM contribution of the free Mn ions when the temperature is lowered (figure 7). This is consistent with the assumption that the anisotropy energy barriers are the main reason for stabilizing the cluster moments. From the temperature dependence of $\chi_{ZFC}(T)$ in the lowest applied fields (figure 1) we calculate the distribution function of the blocking temperatures (equation (B3) in appendix B),

$$F(T) = \frac{1}{\gamma}\frac{\mathrm{d}}{\mathrm{d}T}\left[\frac{T\chi_{ZFC}(T)}{\sigma_s^2(T)}\right] - \alpha. \tag{5}$$

The distribution function, $f(R)$, of the cluster radius, R (or more strictly the radius of the sphere of equivalent volume) is calculated using the relation between the cluster volume and

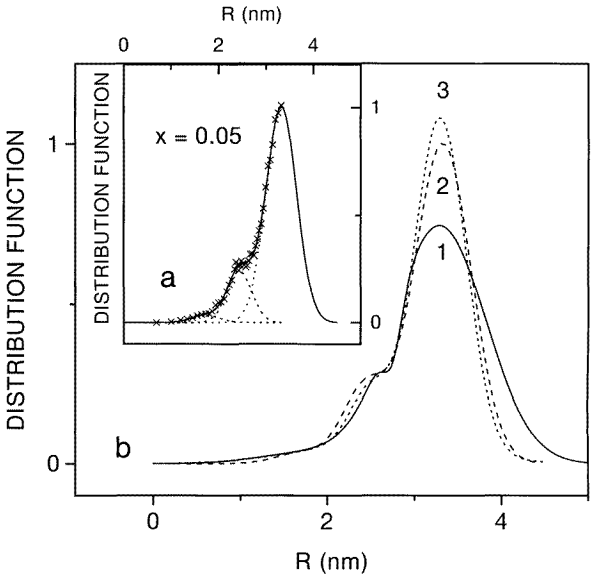

Figure 8. The distribution function of the cluster radius of $Zn_{1-x}Mn_xAs_2$ for $x = 0.01$ (line 1), 0.05 (line 2) and 0.1 (line 3). Inset: composition of the distribution function for the compound with $x = 0.05$ (×) by three overlapping Gaussian distributions.

the blocking temperature given by equation (2) and the dependence of K on T [18]. The constants γ and α are determined by normalizing $f(R)$ to unity and using the condition $f(R) = 0$ at $R = 0$. As evident from figure 8(a) the normalized distribution function for the sample with $x = 0.05$ has a sharp peak at $R_1 \approx 3.3$ nm. Analysis of $f(R)$ with the multiple Gaussian function reveals two other peaks centred at $R_2 \approx 2.4$ nm and $R_3 \approx 1.7$ nm. As follows from figure 8(b) the size distribution functions are similar for all the samples. When x is increased the main peak is sharpened leading to some shift of the cluster sizes towards R_1. The calculated moments at 300 K corresponding to the values of R_1, R_2 and R_3 are $\mu_1 \approx 10.4 \times 10^3\ \mu_B$, $\mu_2 \approx 4.1 \times 10^3\ \mu_B$ and $\mu_3 \approx 1.5 \times 10^3\ \mu_B$, respectively. The average values $\langle R \rangle \approx 3.1$ nm and $\langle \mu \rangle \approx 8.8 \times 10^3\ \mu_B$ are evaluated with the distribution function shown in figure 8(a). The concentration of clusters can be calculated from the equation $N \approx M_s/\sigma_s\langle V \rangle$ where $\langle V \rangle$ is the mean cluster volume. The obtained value $N \approx 1.8 \times 10^{17}$ cm^{-3} corresponds to the mean intercluster distance, $\langle r \rangle = 2(4\pi N/3)^{-1/3} \approx 22$ nm. The cluster parameters found above permit us to compare the scales of the anisotropy energy of a mean cluster, $W_a \approx |K|\langle V \rangle \approx 0.5$ eV ($K \approx -6 \times 10^6$ erg cm^{-3} at 300 K [18]), and of the energy of dipolar interaction, $W_d \approx z_J\langle \mu \rangle^2/\langle r \rangle^3 \approx 0.013$ eV. The long-range character of the dipolar interaction is taken into account by introducing a constant $z_J \approx 33$ stemming from extension of the interaction beyond the nearest neighbours (see comments on equation (A2) in appendix A). Since W_d is less than 3% of W_a the dipolar interaction can be neglected and the description of the magnetic properties of $Zn_{1-x}Mn_xAs_2$ given above is consistent. The difference between the magnetization measured for $B \parallel (100)$ and $B \perp (100)$ does not vanish at $B \approx 50$ kG. On the other hand, the anisotropy field of MnAs is three times lower, $B_a = 18.3$ kG at 300 K [18]. This suggests that the observed anisotropy of the magnetization is connected with some non-sphericity of the cluster shape.

Finally, we discuss the magnetization data assuming that blocking of the cluster moments is caused only by the dipolar interaction between the clusters, i.e. neglecting the influence of the anisotropy energy W_a and the distribution of the cluster sizes. The dependence of M on B for all the specimens can be fitted with equation (4) using the product of VN (since $M_s = \sigma_s VN$) and ξ as adjustable parameters. An example is shown in figure 4, giving $VN = 0.017 \pm 0.001$ (0.020 ± 0.001) and $\xi = 15 \pm 1$ (7 ± 1) for the cases of the parallel (perpendicular) orientation of B with respect to the (100) plane. Hence, the value of ξ differs somewhat from 17.3, predicted by the model of interacting clusters and, additionally, depends on the direction of the magnetic field. The values of V and N can be found separately with equation (3), using those of VN and $T_b \approx 250$ K. This gives the values of $R = 10.9$ nm (10.4 nm), $\mu = 4.6 \times 10^5\ \mu_B$ ($4.0 \times 10^5\ \mu_B$), both at T_b, $N = 3.2 \times 10^{15}$ cm^{-3} (3.7×10^{15} cm^{-3}) and $r = 84$ nm (80 nm). With the values of μ and r above we evaluate $W_a \approx 19.3$ eV (16.8 eV) and $W_d \approx 0.67$ eV (0.55). The value of $W_a \gg W_d$ contradicts with the assumption made in this paragraph that our magnetization data could be explained by attributing the blocking of the cluster moments to the dipolar interactions.

5. Conclusions

In this work the temperature and the field dependences of the magnetization of $Zn_{1-x}Mn_xAs_2$ are investigated for $= 0.01$, 0.05 and 0.1, opening a novel group II–V_2 of DMSs. Analysis of the data gives strong evidence for presence of small MnAs clusters in this compound. The irreversible phenomena observed in $Zn_{1-x}Mn_xAs_2$ starting from $x = 0.01$ reflect the blocking transition in dynamics of the magnetic moments at temperatures comparable with the ferromagnetic Curie temperature of bulk MnAs. The dependence of M on B is consistent with the behaviour of the magnetization below the blocking temperature. The analysis of the temperature dependence of the saturation magnetization demonstrates that the majority of Mn ions in $Zn_{1-x}Mn_xAs_2$ are located in the MnAs clusters. The distribution function of the sizes, the magnetic moments and the concentration of the clusters are obtained. Comparing the anisotropy energy of individual particles and the energy of intercluster dipolar interaction it is concluded on basis of our magnetization data that the anisotropy energy of the clusters is the reason for the blocking of their moments. A dependence of the magnetization on the direction of the applied magnetic field suggests some non-sphericity of the cluster shape.

Appendix A

The blocking of the moments due to the dipolar interaction is a cooperative process similar to freezing of spins in spin-glasses. Therefore, this phenomenon can be analysed in a similar way using the mean-field theory. Following the method proposed in [22] we treat a disordered lattice of interacting cluster moments, μ, in the dipolar approximation, neglecting the distribution of the cluster sizes. Then the equations defining the mean field B_i^* at the ith site may be written as

$$B_i^* = B + \sum_j J_{ij}\mu L\left(\frac{\mu B_j^*}{kT}\right) \tag{A1}$$

where B is the external field, $L(y) = \operatorname{cotanh}(y) - 1/y$ is the Langevin function and $J_{ij} = (1 - 3\cos^2\varphi_{ij})/r_{ij}^3$ are random variables describing the dipolar interaction. Here φ_{ij} is the angle between the direction of the field B_j^* at the site j and the vector distance r_{ij} between the sites i and j. In equation (A1) the summation over the sites j is extended to infinity due to the long-range character of the dipolar interaction. To describe the distribution of the fields

B_i^* we introduce the mean value, $\langle B^* \rangle$, and the variation, $\langle (B^*)^2 \rangle - \langle B^* \rangle^2$, where the angular parenthesis mean the averaging over the configurations. Assuming that the random variables φ_{ij} and R_{ij} in different sites are uncorrelated, we obtain from equation (A1) in a standard way [22] the following relations,

$$\langle B^* \rangle = B + J_0 \langle \mu L(\mu B^*/kT) \rangle \tag{A2}$$

and

$$\langle (B^*)^2 \rangle - \langle B^* \rangle^2 = I_0 \langle \mu^2 L^2(\mu B^*/kT) \rangle. \tag{A3}$$

In equations (A2) and (A3) $J_0 = \sum_j \langle J_{ij} \rangle = -(1/2) \sum_j \langle r_{ij}^3 \rangle = -z_J/r^3$ and $I_0 = \sum_j (\langle J_{ij}^2 \rangle - \langle J_{ij} \rangle^2) = (11/8) \sum_j \langle r_{ij}^6 \rangle = z_I/r^6$. Here $r = 2(4\pi N/3)^{-1/3}$ is the mean distance between the nearest sites, and the values of the constants $z_J \approx 33$ and $z_I \approx 11.6$ are obtained by performing the numerical summation.

The averaging over the configurations in these equations can be made using the Gaussian distribution of fields, $f(B^*) = \exp[-(B^* - B_1)^2/2B_2^2]/[(2\pi)^{1/2} B_2]$, with $B_1 \equiv \langle B^* \rangle$ and $B_2^2 \equiv \langle (B^*)^2 \rangle - \langle B^* \rangle^2$. This gives

$$B_1 = B + \frac{J_0 \mu}{B_2} \int \frac{\mathrm{d}B^*}{\sqrt{2\pi}} \exp\left[- \frac{(B^* - B_1)^2}{2B_2^2} \right] L\left(\frac{\mu B^*}{kT} \right) \tag{A4}$$

and

$$B_2^2 = \frac{I_0 \mu^2}{B_2} \int \frac{\mathrm{d}B^*}{\sqrt{2\pi}} \exp\left[- \frac{(B^* - B_1)^2}{2B_2^2} \right] L^2\left(\frac{\mu B^*}{kT} \right). \tag{A5}$$

It is convenient to analyse the mean-field equations (A4) and (A5) by introducing an analogue of the Edwards–Anderson order parameter, q, and local magnetization, m [22, 23], defined as

$$q = \langle L_2(\mu_B^*/kT) \rangle \quad \text{and} \quad m = \mu \langle L(\mu B^*/kT) \rangle \tag{A6}$$

respectively. They are connected to the parameters B_1 and B_2 by the relations

$$B_1 = B + J_0 m \quad \text{and} \quad B_2^2 = I_0 \mu^2 q \tag{A7}$$

following from equations (A2), (A3) and (A6) and the definition of B_1 and B_2. Replacing B_1 and B_2 in equations (A4) and (A5) with those in equations (A7), and substituting $B^* = B + J_0 m + t\mu(I_0 q)^{1/2}$ we obtain finally the following system of equations for q and m,

$$q = \int \frac{\mathrm{d}t}{\sqrt{2\pi}} \exp\left(- \frac{t^2}{2} \right) L^2 \left[\frac{\mu}{kT} (B + J_0 m + t\mu \sqrt{I_0 q}) \right] \tag{A8}$$

and

$$m = \mu \int \frac{\mathrm{d}t}{\sqrt{2\pi}} \exp\left(- \frac{t^2}{2} \right) L \left[\frac{\mu}{kT} (B + J_0 m + t\mu \sqrt{I_0 q}) \right]. \tag{A9}$$

The macroscopic magnetization is then $M = mN$.

The state of stable moments is defined by $q \neq 0$ and $m = 0$ at $B = 0$. Therefore, this state corresponds to the interval of non-zero solutions of equation (A8) in zero field given by inequality $T \leqslant T_b^{(inter)}$ where

$$T_b^{(inter)} = \mu^2 I_0^{1/2}/3\, k_B. \tag{A10}$$

Since $L(y)$ is a finite function ($L(y) \to 1$ as $y \to \infty$ and $\exp(-t^2/2)$ decays rapidly with increasing t) the expression under the integral in the right-hand side of equation (A9) is determined by small values of t. Therefore, for high fields the third term in the argument of the Langevin function can be neglected, resulting in $m \approx L[\mu(B + J_0 m)/k_B T]$. This

equation is solved in the limits of $\mu B/k_BT \gg 1$ and $B \gg |J_0|m$ taking into account the asymptotic form of the Langevin function, $L(y) \approx 1 - 1/y$ at $y \gg 1$. The solution is given by $m \approx (\mu B + k_BT)/(B + |J_0|\mu)$. For large cluster moments we have then $\mu B \gg k_BT$ resulting in a weak temperature dependence of the magnetization. Finally, the macroscopic magnetization $M = m_N$ can be expressed in the form

$$M \approx \frac{M_s B}{B + \xi M_s} \tag{A11}$$

where $M_s = \mu N$ and $\xi = \pi z_J/6 \approx 17.3$.

Appendix B

The distribution function of the blocking temperatures can be obtained with the following method [24]. The ZFC susceptibility of a system of identical clusters satisfies the conditions $\chi_{ZFC} = \chi_0$ at $T < T_b$ and $\chi_{ZFC} = C/T$ at $T > T_0$, where C is the Curie constant for clusters. The low-field contribution to the susceptibility from the stable clusters is small and depends on T only by σ_s. Then the susceptibility of a system of arbitrary clusters can be written as

$$\chi_{ZFC}(T) = \chi_0 + \frac{C}{T}\int_0^T F(T^*)\,\mathrm{d}T^* \tag{B1}$$

where the first and the second terms on the right-hand side represent the contributions of the stable and the SP clusters, respectively, and $F(T)$ is the distribution function of the blocking temperatures. It is convenient to represent the parameters χ_0 and C as $\chi_0 = \gamma\alpha\sigma_s^2$ and $C = \gamma\sigma_s^2$ (where α and γ are constants) depending on T only by the temperature dependence of σ_s. Then equation (B1) can be written in the form

$$\chi_{ZFC}(T) = \gamma\sigma_s^2\left[\alpha + \frac{1}{T}\int_0^T F(T^*)\,\mathrm{d}T^*\right]. \tag{B2}$$

Finally, $F(T)$ can be given in the form

$$F(T) = \frac{1}{\gamma}\frac{\mathrm{d}}{\mathrm{d}T}\left(\frac{\chi_{ZFC}T}{\sigma_s^2}\right) - \alpha \tag{B3}$$

obtained by differentiation of equation (B2) with respect to T. The values of the constants γ and α can be determined by normalizing $F(T)$ to unity and using the condition $F(T) = 0$ at $T = 0$, respectively.

References

[1] Furdyna J K and Kossut J (eds) 1988 *Semiconductors and Semimetals* vol 25 (London: Academic)

[2] Brandt N B and Moshchalkov V V 1984 *Adv. Phys.* **33** 193

[3] Denissen C J M, Nishihara H, van Gool J C and de Jonge W J M 1986 *Phys. Rev.* B **33** 7637

[4] Denissen C J M, Sun Dakun, Kopinga K, de Jonge W J M, Nishihara H, Sakakibara T and Goto T 1987 *Phys. Rev.* B **36** 5316

[5] Laiho R, Lashkul A V, Lähderanta E, Säisä L and Zakhvalinskii V S 1990 *Proc. 20th Int. Conf. on the Physics of Semiconductors (Thessaloniki, 1990)* vol 1, ed E M Anastassakis and J D Joannopoulos (Singapore: World Scientific) p 759

Lashkul A V, Lähderanta E, Laiho R and Zakhvalinskii V S 1992 *Phys. Rev.* B **46** 6251

[6] Laiho R, Lashkul A, Lähderanta E, Mäkinen A and Zakhvalinskii V S 1992 *Solid State Commun.* **83** 375

[7] Lähderanta E, Laiho R, Lashkul A V, Mäkinen A and Zakhvalinskii V S 1993 *Semicond. Sci. Technol.* **8** S37

[8] Laiho R, Lashkul A V, Lähderanta E, Lisunov K G, Stamov V N and Zakhvalinskii V S 1995 *J. Phys.: Condens. Matter* **7** 7629

[9] Laiho R, Lisunov K G, Stamov V N and Zakhvalinskii V S 1996 *J. Phys. Chem. Solids* **57** 1

[10] Laiho R, Lisunov K G, Lähderanta E, Stamov V N and Zakhvalinskii V S 1997 *J. Appl. Phys.* **81** 5115
[11] Lazarev V B, Shevchenko V Ya, Grinberg Ya N and Sobolev V V 1988 *Semiconductor Compounds of II–V Group* (Moscow: Nauka)
[12] Fleet M 1974 *Acta Crystallogr.* B **30** 122
[13] Ugai Ya A and Zyubina T A 1966 *Neorgan. Mater.* **2** 9
[14] Turner W J, Fishler A S and Reese W E 1961 *Phys. Rev.* **121** 759
[15] Marenkin S F, Lazarev V B, Shevchenko V Ya and Sokolovsky K A 1980 *J. Crystal Growth* **50** 761
[16] Pytlik L and Zieba A 1985 *J. Magn. Magn. Mater.* **51** 199
[17] Ohto H, Munekata H, von Molnar S and Chang L L 1991 *J. Appl. Phys.* **69** 6103
[18] De Blois R W and Rodbell D S 1963 *J. Appl. Phys.* **34** 1101
[19] Bean C P and Livingston J D 1959 *J. Appl. Phys.* **30** 120S
[20] Berkowitz A E, Mitchell J R, Carey M J, Young A P, Rao D, Starr A, Zhang S, Spada F E, Parker F T, Hutten A and Thomas G 1993 *J. Appl. Phys.* **73** 5320
[21] Pekarek T M, Crooker B C, Nolte D D, Deak J, McElfresh M, Chang J C P, Harmon E S, Melloch M R and Woodal J M 1997 *J. Magn. Magn. Mater.* **169** 261
[22] Ginzburg S L 1989 *Irreversible Phenomena of Spin Glasses* (Moscow: Nauka)
[23] Chowdhury D 1986 *Spin Glasses and Other Frustrated Systems* (Singapore: World Scientific)
[24] Wohlfarth E P 1979 *Phys. Lett.* **70A** 489